Nano Research

Open Access

Research Article

Mitochondria replenishment enhances senescent periodontal ligament stem cell osteogenesis and facilitates bone repair

Gaoshaer Nuerlan[1,2], Min Yu[3], Xiangyao Wang[1,2], Yuxiao Zhang[1,2], Yuanyuan Li[1,2], Kehan Zhang[1,2], Lin Pan[1,2], Ahsawle Ozathaley[1,2], Yaxin Wu[1,2], Qilin Li[1,2], Jing Mao[1,2] ✉, Yan Liu[3] ✉, and Shiqiang Gong[1,2] ✉

[1] *Center of Stomatology, Tongji Hospital, Tongji Medical College, Huazhong University of Science and Technology, Wuhan 430030, China*
[2] *School of Stomatology, Tongji Medical College, Huazhong University of Science and Technology & Hubei Province Key Laboratory of Oral and Maxillofacial Development and Regeneration, Wuhan 430022, China*
[3] *Central Laboratory, Peking University School and Hospital for Stomatology, Beijing 100081, China*

Cite this article: *Nano Research*, **2025**, *18*, 94907375. https://doi.org/10.26599/NR.2025.94907375

ABSTRACT: Aging is characterized by the progressive accumulation of molecular and cellular damage, leading to disrupted bone homeostasis and reduced osteogenic potential. Mitochondrial dysfunction, a hallmark of aging, results in elevated reactive oxygen species levels and reduced mitochondrial membrane potential, which significantly impairs osteogenesis of osteoprogenitors cells. Inspired by the naturally occurring intercellular mitochondria transfer during tissue healing process, which activates and enhances cellular reparative functions, this study investigated whether mitochondria replenishment could restore osteogenic capacity of aged human periodontal ligament stem cells (hPDLSCs) and promote bone defect repair. Our findings demonstrate that mitochondria replenishment effectively restores mitochondrial function, enhances osteogenic differentiation of aged hPDLSCs, as well as facilitates bone defect repair *in vivo*. Mechanistically, mitochondria supplementation upregulates the mitochondrial anchoring protein A-kinase anchoring protein 1 (AKAP1) and activates the cAMP/PKA signaling pathway in mitochondria-receipient hPDLSCs. This study underscores the therapeutic potential of mitochondrial supplementation in reversing aging-related impairments in hPDLSCs and identifies the AKAP1-regulated cAMP/PKA pathway as a key mechanism. These findings offer a promising strategy for overcoming aging-associated challenges in bone regeneration.

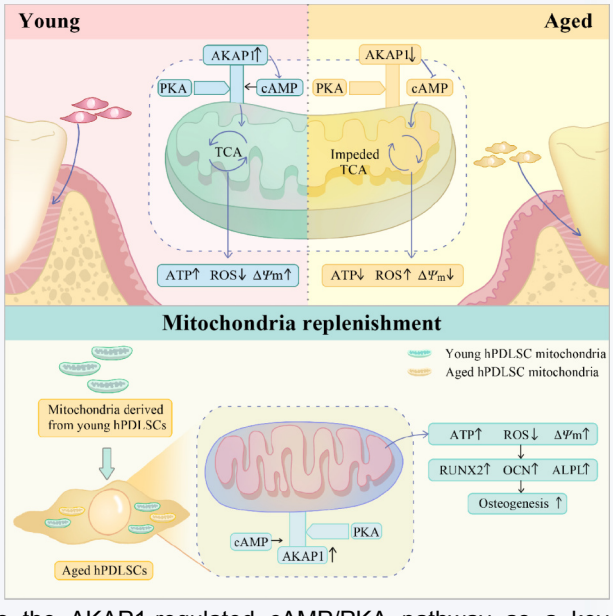

KEYWORDS: mitochondria replenishment, aging, human periodontal ligament stem cells (hPDLSCs), osteogenic differentiation, cAMP/protein kinase A (PKA) signaling

1 Introduction

The rapid growth of the aging population has led to an increasing demand for the regeneration of oral, periodontal, and craniofacial tissues, posing significant challenges to regenerative medicine [1–4]. In this context, stem cell-based regenerative approaches, synergistically combined with biomaterial-mediated technologies, have emerged as key pivotal therapeutic strategies in modern osseous regeneration research [5, 6]. However, a major challenge remains in preserving the differentiation potential and proliferative capacity of stem cells [7–9]. However, aging inevitably diminishes the availability and proliferation of stem cells in the microenvironment of bone metastasis [10, 11]. Despite of characteristics such as cell turnover that can mitigate aging-related damage, the proliferative capacity and number of stem cells nonetheless exhibit varying degrees of decline with aging [12, 13]. Human periodontal ligament stem cells (hPDLSCs) are considered ideal seed cells for tissue regeneration due to their self-renewal

Received: February 12, 2025; **Revised:** March 10, 2025
Accepted: March 14, 2025

✉Address correspondence to Jing Mao, maojing@hust.edu.cn; Yan Liu, orthoyan@bjmu.edu.cn; Shiqiang Gong, gsq@hust.edu.cn

capability, multilineage differentiation potential, and immunomodulatory effects [14]. Similarly, studies found that the proliferative capacity, migratory potential, and osteogenic ability of hPDLSCs diminished as age increased [15]. Therefore, there is an urgent need to implement effective strategies to counteract the age-related decline in stem cell function in aging individuals, thereby enhancing the therapeutic outcomes for bone defects.

Mitochondria serve as the central hub for energy metabolism in organisms, regulating a wide array of metabolic pathways including adenosine triphosphate (ATP) synthesis, amino acid biosynthesis, and fatty acid metabolism [16]. In addition to serving as cellular powerhouses, mitochondria are crucial regulators of intracellular and intercellular signaling pathways. They also help maintain cellular homeostasis by regulating cell fates and redox balance [17, 18]. Mitochondrial dysfunction has been implicated in the pathogenesis of various diseases, including pulmonary fibrosis [19], tendinopathy [20], and osteoporosis [21]. In senescent cells, mitochondrial function deteriorates due to accumulated oxidative damage, characterized by compromised mitochondrial DNA (mtDNA) integrity, diminished mitochondrial membrane potential ($\Delta\Psi_m$), and elevated levels of reactive oxygen species (ROS). These result in reduced ATP production and impaired antioxidant defense mechanisms [22, 23]. This decline in mitochondrial function not only exacerbates tissue degeneration but also compromises cellular regenerative capacity. Therefore, restoring the mitochondrial functions is a critical step to rejuvenate aged stem cells for tissue repair.

Mitochondrial dysfunction has been identified as a key contributor to diseases such as alzheimer's disease (AD) [24], cardiac failure [25], and tendinopathy [20]. Mitochondria dysfunction is a risk for aging process, including the continuous mtDNA mutations and the increased accumulation of ROS [26]. When tissues or organs undergo stress or injury, spontaneously intercellular mitochondria transfer occurs to rescue the regenerative or protective functions of cells. Inspired by the natural phenomena occurring in the human body during tissue healing, mitochondria replenishment has emerged as a novel therapeutic strategy, whereby functional mitochondria are delivered to damaged or senescent cells to restore cellular function, a process termed mitochondrial supplementation therapy [27, 28]. Studies have shown that mitochondria replenishment can restore impaired mitochondrial function, thereby offering a promising therapeutic approach for these conditions. Despite the demonstrated therapeutic potential of mitochondria replenishment in various conditions, its application in restoring the osteogenic differentiation of aged stem cells remains unexplored, and the underlying molecular mechanisms require further investigation.

In this study, we demonstrate that transplantation of youthful mitochondria from young hPDLSCs to aged hPDLSCs restores mitochondrial function and osteogenic differentiation ability. Mechanistically, mitochondria replenishment reduces cellular ROS production and restores mitochondrial $\Delta\Psi_m$ by activating the cAMP/protein kinase A (PKA) signaling pathway of recipient cells. This study provides direct evidence supporting the feasibility of mitochondria replenishment as a therapeutic strategy to rejuvenate aged hPDLSCs and promotes bone defect repair (Fig. 1).

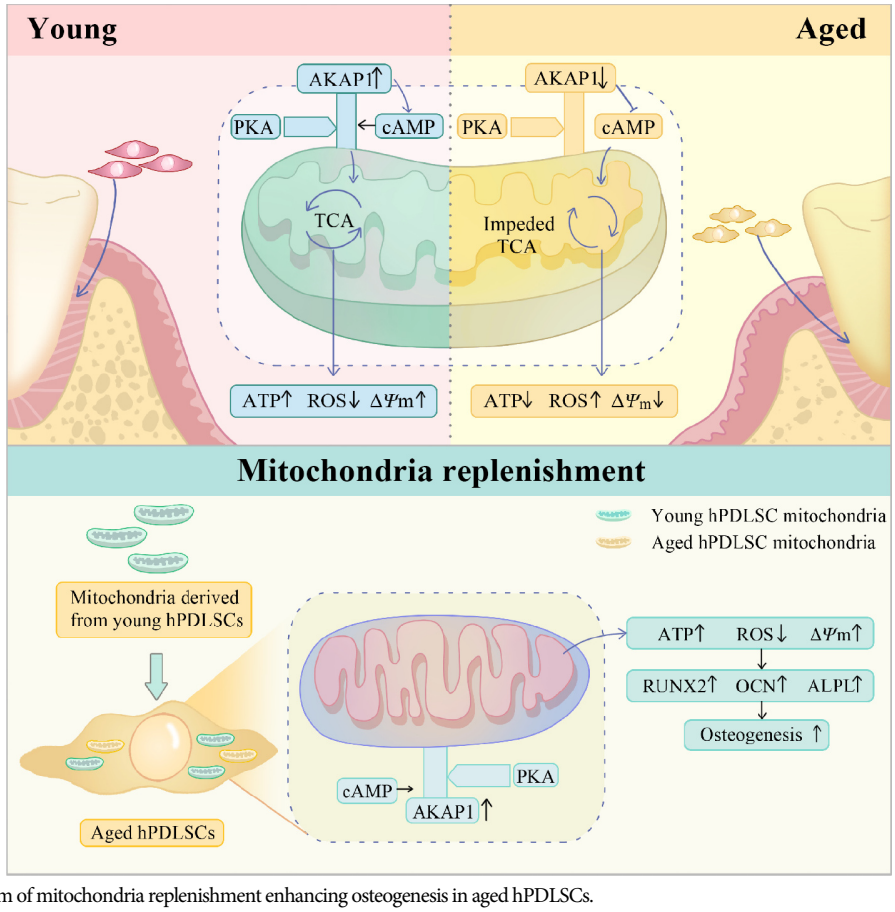

Figure 1 Schematic diagram of mitochondria replenishment enhancing osteogenesis in aged hPDLSCs.

2 Results

2.1 Aging causes maxillary alveolar bone (AB) loss and impairs osteogenesis in the periodontium of mice

To investigate the differences in maxillary bone mass between young and aged mice, we harvested the maxillae from 8-week-old and 15-month-old C57BL/6 mice. Subsequently, micro-computed tomography (Micro-CT) was employed to assess periodontal alveolar bone mass-related parameters including bone volume/total volume (BV/TV), trabecular thickness (Tb.Th), trabecular number (Tb.N), and trabecular separation (Tb.Sp). The results demonstrated an apparent diminution of maxillary bone mass in the aged mice (Figs. 2(a)–2(e)). Immunofluorescence co-localization and immunohistochemistry for osteogenesis-related markers in the periodontium of aged mice including osteopontin (OPN), Runt-related transcription factor 2 (RUNX2), and osteocalcin (OCN), along with CD146, a specific marker for stem cells, provided corroborative evidence, supporting the phenomenon that osteogenesis of stem cells was impaired in the periodontium of aged mice (Figs. 2(f)–2(l)).

2.2 Aging impairs cell proliferation, mitochondrial function and osteogenic differentiation in hPDLSCs

We isolated stem cells from human periodontal ligament tissue under the guidance of a well-established protocol [29, 30] and conducted osteogenic, chondrogenic, and adipogenic differentiation induction to confirm the multipotency of hPDLSCs. After osteogenic induction for 21 days, hPDLSCs exhibited calcified nodule formation (Fig. S1(a) in the Electronic Supplementary Material (ESM)). After chondrogenic induction for 21 days, cells aggregated into clusters and stained blue (Fig. S1(b) in the ESM). Following 21 days of adipogenic induction, lipid droplets accumulated within the cells (Fig. S1(c) in the ESM). These findings confirmed that cultured hPDLSCs possess mesenchymal stem cells-like characteristics with multi-lineage differentiation potential. To establish an aging model of hPDLSCs, we carried out serial passage and selected the third and fifteenth-passage hPDLSCs for further analysis [31–33]. We performed γH2AX DNA damage staining, senescence β-galactosidase staining, and western blotting detection of aging markers P16, P21. The results demonstrated successful construction of the aging model of hPDLSCs (Figs. S2(a)–S2(d) in the ESM).

To further elucidate functional differences between young and aged hPDLSCs, we conducted EdU assays, which revealed decreased proliferative capacity in aged hPDLSCs compared to young hPDLSCs (Figs. 3(a) and 3(b)). Exhibited by RT-qPCR and Western blot (WB), the expression levels of osteogenic-related genes (*OCN*, *COL-I*, *RUNX2*) and proteins (COL-I, ALPL, RUNX2) were definitely lower in aged hPDLSCs than in young cells (Figs. 3(c)–3(g)). Alkaline phosphatase (ALP) staining and alizarin red staining (ARS) staining also showed impaired osteogenic differentiation in aged hPDLSCs (Figs. 3(h)–3(k)).

Given that mitochondrial dysfunction is a hallmark of cellular aging [34], we hypothesized that mitochondrial dysfunction might contribute to the reduced osteogenic differentiation of aged hPDLSCs. Transmission electron microscopy (TEM) revealed normal mitochondrial morphology with continuous outer membranes and intact structures in young hPDLSCs, whereas aged hPDLSCs exhibited swollen mitochondria with blurred cristae (Figs. 3(l) and 3(m)). JC-1 staining indicated decreased $\Delta\Psi_m$ in aged cells (Figs. 3(n) and 3(o)), while ROS levels were significantly elevated (Figs. 3(p) and 3(q)). Collectively, these results indicated that mitochondrial dysfunction might interpret the diminished osteogenic ability of aged hPDLSCs.

2.3 Mitochondria replenishment restores osteogenic and mitochondrial function in aged hPDLSCs

In previous studies, it has been reported that mitochondria replenishment can contribute to the proliferation, migration, and osteogenic potential of bone marrow mesenchymal stem cells (BMSCs) [35, 36]. However, whether mitochondria replenishment could rejuvenate aged stem cells (e.g., hPDLSCs) and recover the osteogenic differentiation capacity of aged hPDLSCs remains unknown. TOMM20 is a mitochondrial import receptor involved in the recognition and translocation of precursor proteins into mitochondria, which serves as an important marker of mitochondrial integrity [37]. Therefore, we labeled the mitochondria of young hPDLSCs with TOMM20-GFP and extracted them using differential centrifugations. These mitochondria were then co-cultured with aged hPDLSCs labeled with MitoTracker Deep Red for 30 min, 3, 6, and 9 h. High-resolution confocal microscopy confirmed the successful transfer of young hPDLSCs-derived mitochondria into aged hPDLSCs (Figs. 4(a)–4(c)).

Subsequently, we examined whether the transferred mitochondria from young hPDLSCs could modulate mitochondrial function and osteogenic differentiation of aged hPDLSCs. The results demonstrated that aged hPDLSCs receiving young hPDLSCs-derived mitochondria (Aged hPDLSCs + Mito(Y)) exhibited significantly enhanced mitochondrial function, reduced ROS levels (Figs. 5(a) and 5(b)), and restored $\Delta\Psi_m$ (Figs. 5(c) and 5(d)). Additionally, the expressions of osteogenic-related genes (*OCN*, *COL-I*, *RUNX2*) and proteins (COL-I, ALPL, RUNX2) were markedly upregulated (Figs. 5(e)–5(i)). ALP and ARS staining further corroborated the recovery of osteogenic capacity (Figs. 5(j)–5(m)). Collectively, these findings indicate that the mitochondrial function and osteogenic differentiation ability of aged hPDLSCs were significantly improved following the transplantation of mitochondria from young hPDLSCs. This study provides evidence supporting the feasibility of mitochondrial supplementation therapy as a potential approach to reverse the functional decline of aged hPDLSCs.

2.4 Mitochondria replenishment activates the A-kinase anchoring protein 1 (AKAP1)-regulated cAMP/PKA pathway

To further elucidate the effects of mitochondria replenishment on aged hPDLSCs and to identify the underlying molecular mechanisms, we conducted RNA sequencing (RNA-seq) analysis on Young, Aged, and Aged + Mito(Y) hPDLSCs (Fig. 6). Principal component analysis (PCA, $P \leq 0.05$) revealed significant transcriptional differences among the three groups (Fig. 6(a)). We then screened for genes that were downregulated in Aged hPDLSCs compared to Young hPDLSCs, and recovered in Aged + Mito(Y) hPDLSCs, and focused on mitochondrial-related genes based on the MitoCarta 3.0 database among these genes. This screening strategy identified 26 differentially expressed genes (DEGs) (Fig. 6(b)), as illustrated by the volcano plot (Fig. 6(c)). We selected

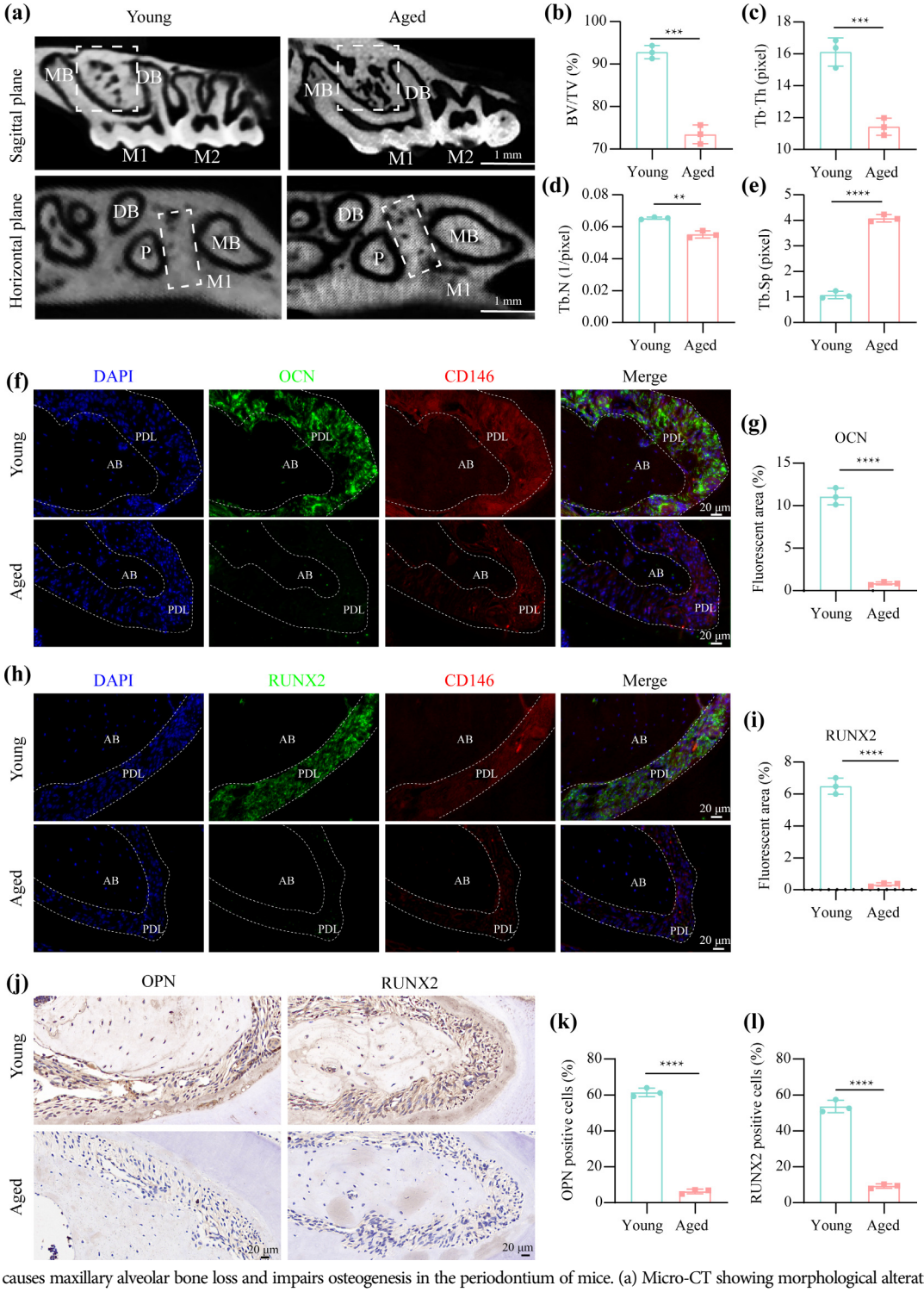

Figure 2 Aging causes maxillary alveolar bone loss and impairs osteogenesis in the periodontium of mice. (a) Micro-CT showing morphological alterations of maxillary alveolar bone images (two-dimensional images) in young and aged mice (M1 refers to the maxillary first molar; M2 refers to the maxillary second molar; MB refers to mesial-buccal root; DB refers to disto-buccal root; P refers to palatine root). (b) Quantitative analyses of bone volume fraction (BV/TV (%)). (c) Quantitative analyses of trabecular thickness (Tb.Th). (d) Quantitative analyses of trabecular number (Tb.N). (e) Quantitative analyses of Trabecular Separation (Tb.Sp). (f)–(i) Immunofluorescence staining and statistical results showing the osteogenic markers (OCN, RUNX2) and the stem cell marker (CD146) in PDL and AB sections from young and aged mice. (j)–(l) Immunohistochemical staining and statistical results showing the number of OPN^+ and $RUNX2^+$ cells in AB and PDL sections from young and aged mice. ** $P < 0.01$, *** $P < 0.001$ and **** $P < 0.0001$.

the top ten differentially expressed genes for subsequent RT-qPCR validation, which corroborated the RNA-seq results. Among these, *AKAP1* exhibited the most pronounced expression difference before and after mitochondria replenishment. Besides, *AKAP1* exhibited the highest gene expression level in Aged hPDLSCs + Mito(Y) compared to the other nine genes (Fig. 6(d)). This further confirmed that *AKAP1* was significantly upregulated in Aged+Mito(Y) hPDLSCs.

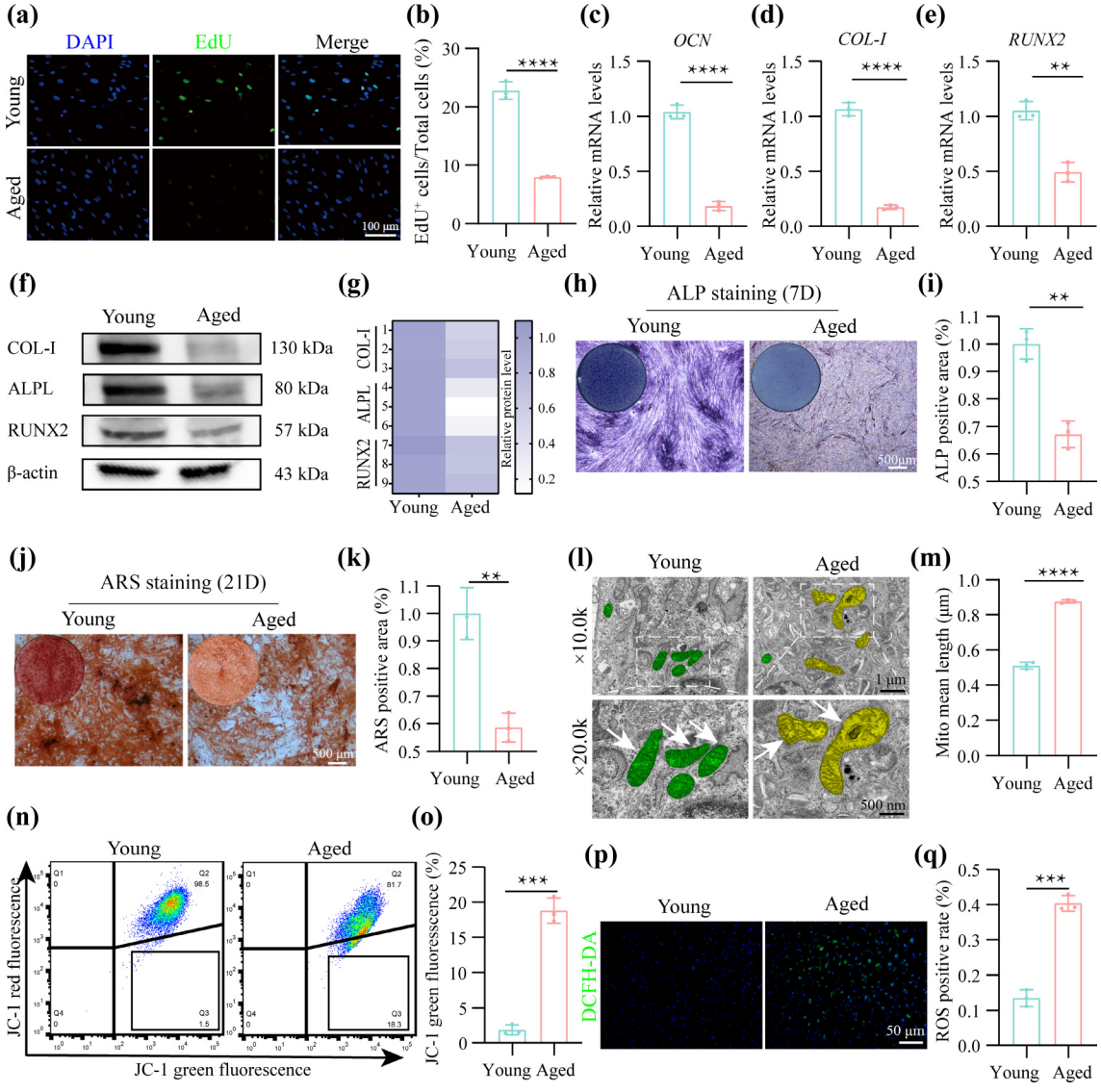

Figure 3 Aging impairs cell proliferation, mitochondrial function and osteogenic differentiation in aged hPDLSCs. (a) and (b) EdU staining and statistical results showing cell proliferation activity of young and aged hPDLSCs (blue: nuclei; green: EdU; scale bar = 100 μm). (c)–(e) RT-qPCR results show the relative mRNA expression of *OCN* , *COL-I* and *RUNX2* in young and aged hPDLSCs groups. (f) and (g) Western blot analysis showing relative protein expression of COL-I, ALPL, RUNX2, and β-actin in young and aged hPDLSCs. (h) ALP staining after osteogenic induction for 7 days in the young and aged hPDLSCs groups. (i) Semi-quantitative analysis of ALP staining. (j) ARS staining after osteogenic induction for 21 days in the young and aged hPDLSCs groups. (k) Semi-quantitative analysis of ARS staining. (l) and (m) TEM images showing mitochondrial morphology in young and aged hPDLSCs, with mitochondrial length quantification (white arrows: mitochondria; green: young mitochondria; yellow: aged mitochondria). (n) JC-1 flow cytometry analysis showing mitochondrial membrane potential in young and aged hPDLSCs (Q2: high potential; Q3: low potential). (o) Semiquantification of (n). (p) and (q) Immunofluorescence staining and statistical results showing intracellular ROS levels in young and aged hPDLSCs (blue: nuclei; green: ROS). ** $P < 0.01$, *** $P < 0.001$ and **** $P < 0.0001$.

AKAP1 is a mitochondrial PKA anchoring protein that is essential for maintaining mitochondrial homeostasis and cell viability [38]. Therefore, we propose that AKAP1 plays an essential role in bone regeneration through mitochondria replenishment. Gene Ontology (GO) enrichment analysis indicated that the upregulated genes were primarily enriched in pathways related to regulation of mitochondrial fusion, mitochondrial fusion, mitochondrial transport, and bone development (Fig. 6(e)). Previous study has shown that AKAP1 can tether PKA to the outer mitochondrial membrane (OMM), facilitating localized cAMP signaling [39]. AKAP1-regulated cAMP/PKA signaling promotes the maintenance of mitochondrial homeostasis [40]. Supportively, gene set enrichment analysis (GSEA) also confirmed the significant enrichment in cAMP/PKA signaling pathways (Figs. 6(f) and 6(g)). To further elucidate the role of the AKAP1/PKA pathway, we investigated the impact of AKAP1 knockout on PKA activity. As illustrated in Fig. S6 in the ESM, the results demonstrated that PKA activity was markedly diminished following AKAP1 knockout. Therefore, we conducted JC-1 flow cytometry and ALP staining to examine the impact of AKAP1 on mitochondrial function and osteogenic differentiation. As illustrated in Fig. S5 in the ESM, following AKAP1 knockdown, both the mitochondrial membrane potential and osteogenic differentiation capacity were significantly reduced. WB analysis further confirmed that the expression of AKAP1 protein was significantly higher in Aged + Mito(Y) hPDLSCs compared to Aged hPDLSCs, indicating that the

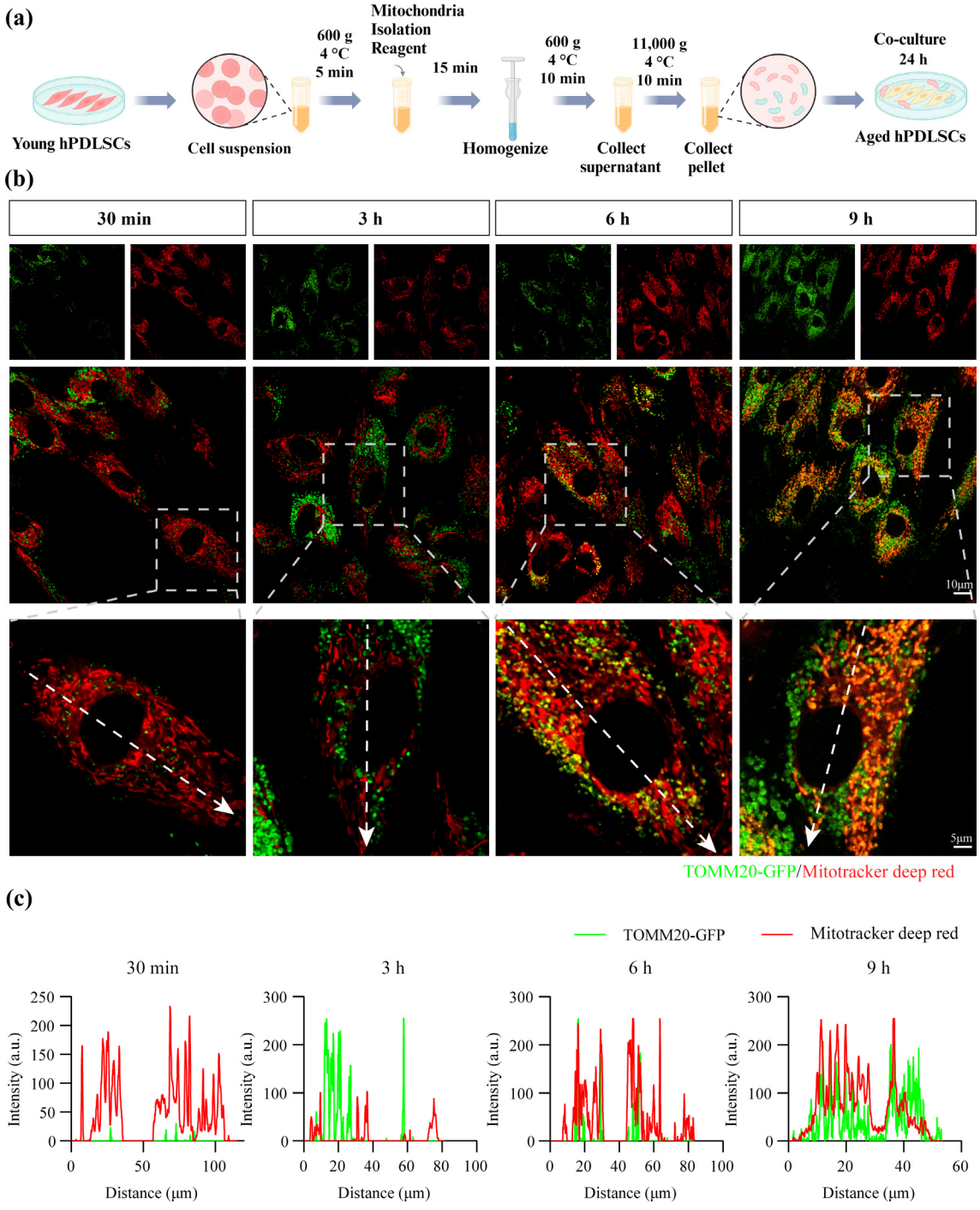

Figure 4 Mitochondria replenishment process. (a) Schematic of the mitochondria replenishment process. (b) High-resolution confocal microscopy images of mitochondria replenishment in hPDLSCs (green: TOMM20-GFP; red: Mitotracker Deep Red). (c) Intensity trace along the dotted white arrow shown in (b).

increased AKAP1 expression contributed to the rejuvenating effect of Mitochondria replenishment on aged hPDLSCs (Figs. 6(h) and 6(i)).

2.5 Mitochondria replenishment enhances calvarial bone regeneration in rats

To assess the *in vivo* efficacy of mitochondria replenishment, we utilized calvarial defect models in rats (diameter = 5 mm) to assess the bone regeneration potentials of mitochondria replenishment (Fig. 7(a)). Young, Aged, Aged + Mito(Y) hPDLSCs, and Aged + shAKAP1Mito(Y) hPDLSCs (transfer young hPDLSCs mitochondria with the AKAP1 gene knocked out into senescent hPDLSCs) were loaded onto IMC/ZnO scaffolds at a density of 5×10^5 cells per scaffold [41]. After 4 and 8 weeks of repair, rat calvarial samples were collected for micro-CT, HE staining, Masson staining, immunohistochemistry, and immunofluorescence analyses. The micro-CT results demonstrated that the blank group exhibited the least bone formation, followed by the scaffold only group. In contrast, both the Young hPDLSCs group and the scaffold + Aged + Mito(Y) hPDLSCs group showed enhanced new bone formation

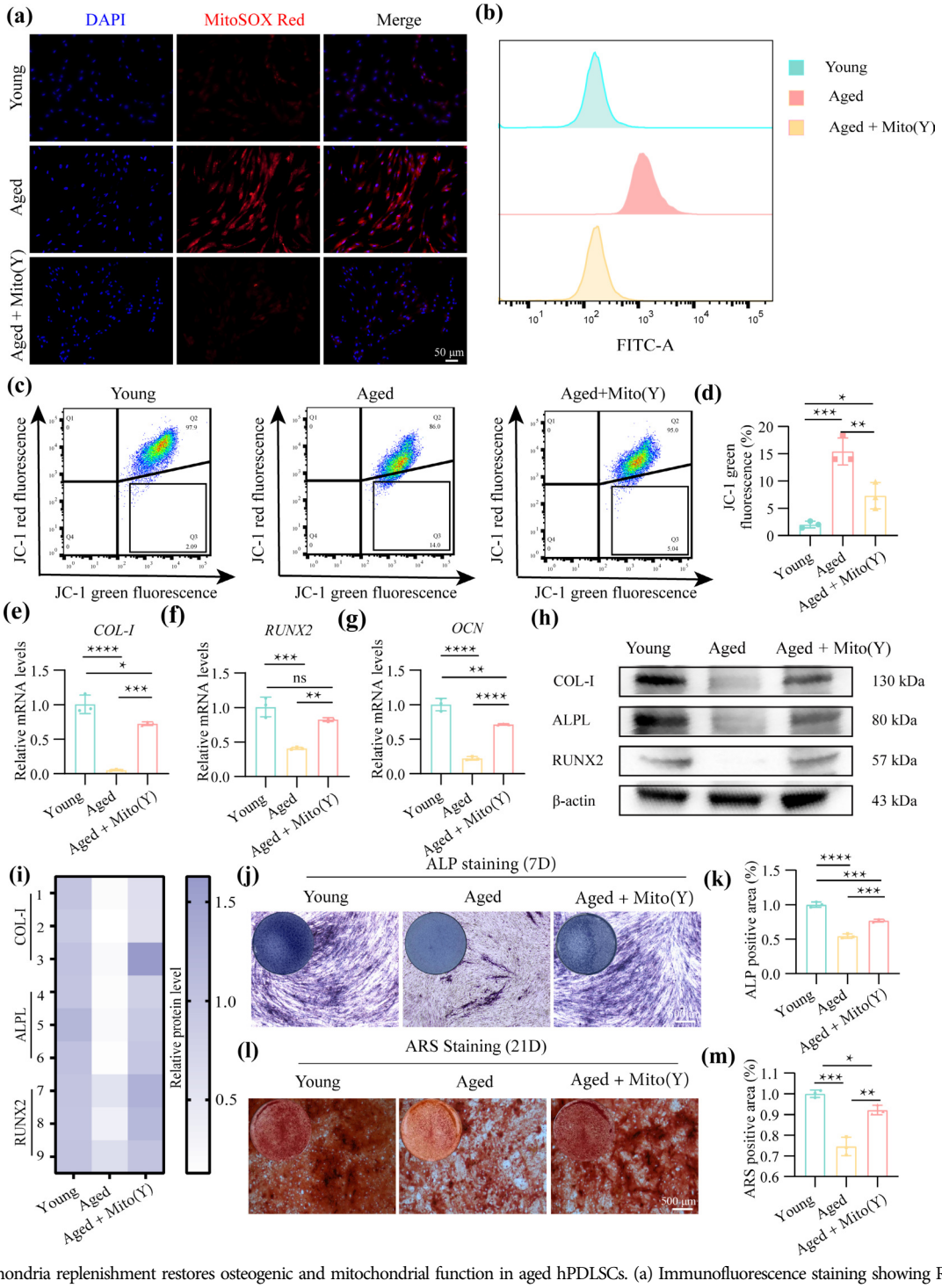

Figure 5 Mitochondria replenishment restores osteogenic and mitochondrial function in aged hPDLSCs. (a) Immunofluorescence staining showing ROS levels in the Young, Aged, and Aged + Mito(Y) hPDLSCs (red: MitoSOX; blue: nuclei). (b)ROS flow cytometry analysis results showing intracellular ROS levels in Young, Aged, and Aged + Mito(Y) hPDLSCs. (c) JC-1 flow cytometry analysis results showing mitochondrial membrane potential in the Young, Aged, and Aged + Mito(Y) hPDLSCs (Q2: high potential; Q3: low potential). (d) Semiquantification of (c). (e)–(g) Relative mRNA expressions of *OCN* , *COL-I*, and *RUNX2* in the Young, Aged, and Aged + Mito(Y) hPDLSCs. (h)–(i) Western blot of COL-I, ALPL, RUNX2, and β-actin in Young, Aged, and Aged + Mito(Y) hPDLSCs. (j) ALP staining after osteogenic induction for 7 days in the Young, Aged, and Aged+Mito(Y) hPDLSCs. (k) Semiquantitative analysis of ALP staining. (l) ARS staining after osteogenic induction for 21 days in the Young, Aged, and Aged + Mito(Y) hPDLSCs. (m) Semiquantitative analysis of ARS staining. ns means no significance. * $P < 0.05$, ** $P < 0.01$, *** $P < 0.001$ and **** $P < 0.0001$.

emerged at both the defect margins and central regions. Conversely, the scaffold + Aged + shAKAP1 Mito(Y) hPDLSCs group, in which AKAP1 was knocked down, exhibited significantly reduced new bone formation (Fig. 7(b)). As shown in Fig. 7(c), the BV/TV values of the scaffold + Young hPDLSCs group (41.57% ± 4.34% at week 4, 55.70% ± 4.12% at week 8) and the scaffold + Aged + Mito(Y) hPDLSCs group (39.85% ± 3.71% at week 4, 45.92% ± 5.22% at week 8) were significantly higher compared to the other groups. In

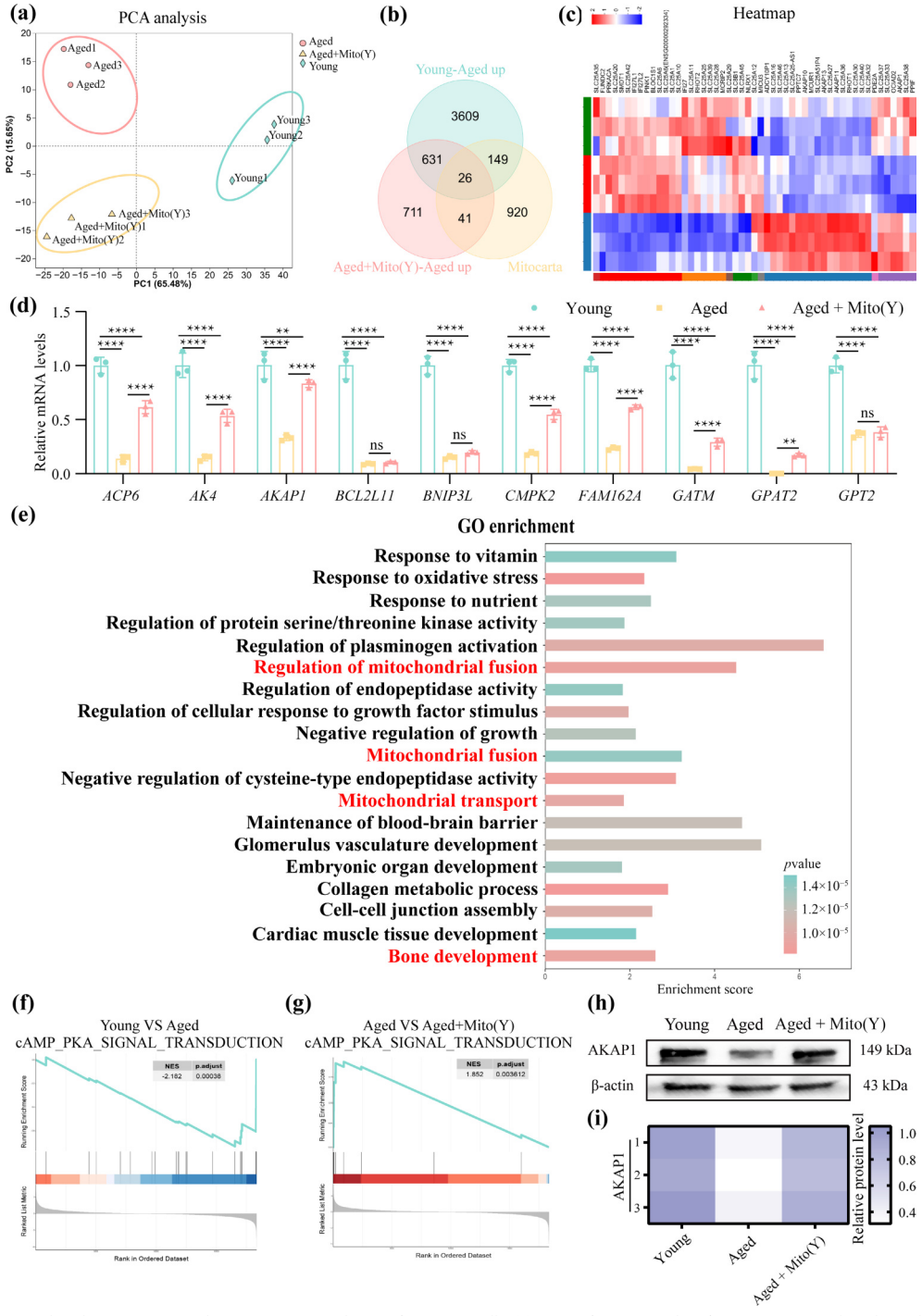

Figure 6 Mitochondria replenishment activates the cAMP/PKA pathway of recipient cells. (a) PCA of RNA-seq data from Young, Aged, and Aged + Mito(Y) hPDLSCs. (b) Venn diagram showing the overlap between DEGs and mitochondria-related genes from the MitoCarta3.0 database. (c) Heatmap of mitochondrial biogenesis-related gene expression (qPCR) comparing Young vs. Aged hPDLSCs and Aged vs. Aged + Mito(Y) hPDLSCs. (d) Relative mRNA expression of the top 10 DEGs. (e) GO enrichment analysis comparing Young vs. Aged hPDLSCs and Aged vs. Aged+Mito(Y) hPDLSCs. (f) GSEA of cAMP/PKA signaling pathways in Young vs. Aged hPDLSCs ($P < 0.001$, NES = −2.182). (g) GSEA of cAMP/PKA signaling pathways in Aged vs. Aged + Mito(Y) hPDLSCs ($P < 0.01$, NES = 1.852). (h) and (i) Western blot exhibits relative protein expressions of AKAP1, with β-actin in Young, Aged, and Aged + Mito(Y) hPDLSCs. ns means no significant. * $P < 0.05$, ** $P < 0.01$, *** $P < 0.001$ and **** $P < 0.0001$.

contrast, the BV/TV value of the scaffold + Aged + shAKAP1 Mito(Y) hPDLSCs group (23.25% ± 3.57% at week 4, 26.55% ± 5.74% at week 8), in which AKAP1 was knocked down, was significantly lower. Quantitative analysis of Tb.Th, and Tb.N showed similar results, the scaffold + Young hPDLSCs group exhibited the highest values, followed by the scaffold + Aged + Mito(Y) hPDLSCs group, with the blank control group having the lowest values (Figs. 7(d) and 7(e)). Conversely, Tb.Sp results were inversely correlated (Fig. 7(f)).

To characterize the regenerated calvarial bone structure, we

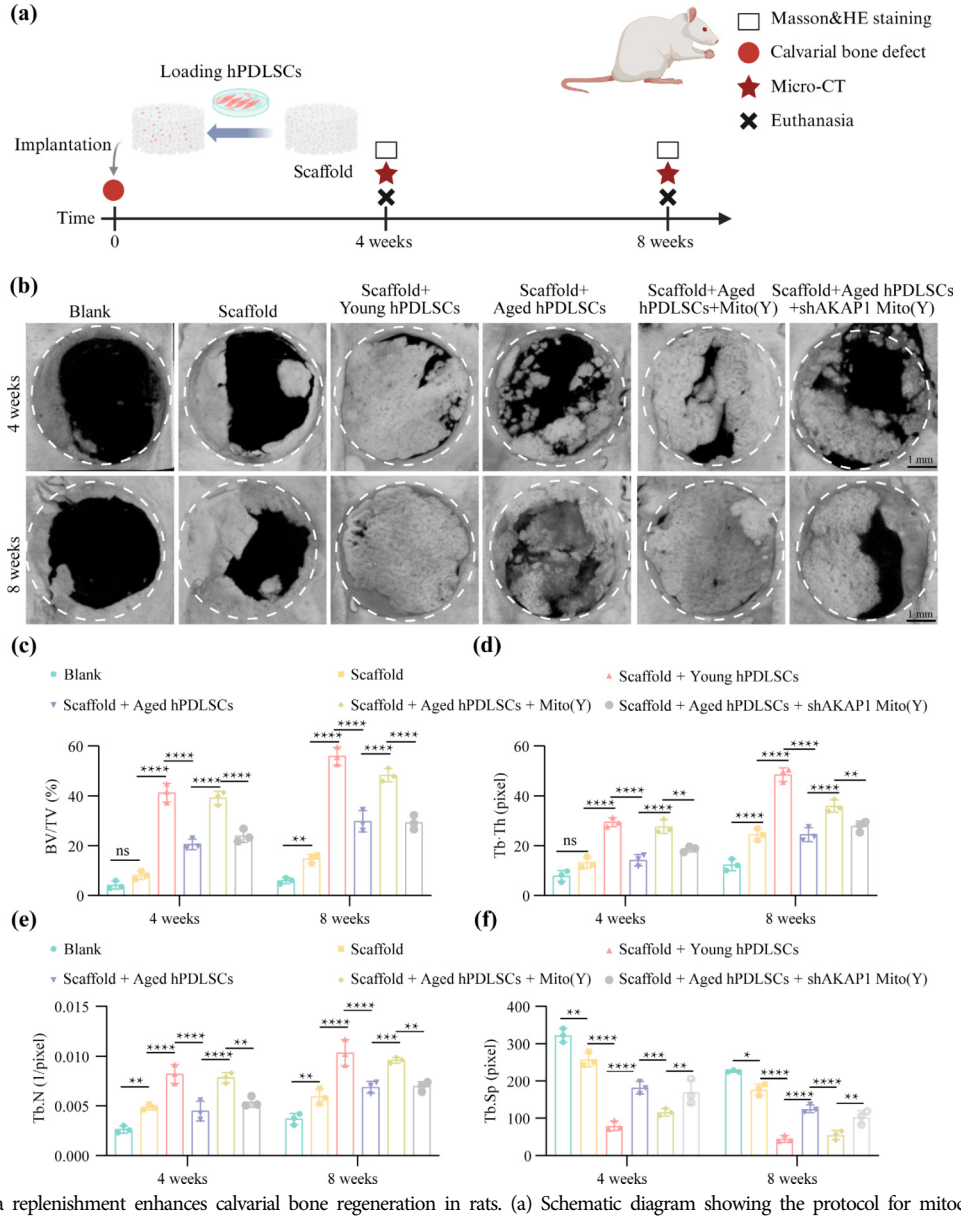

Figure 7 Mitochondria replenishment enhances calvarial bone regeneration in rats. (a) Schematic diagram showing the protocol for mitochondria replenishment promotes calvarial bone regeneration. (b) Representative micro-CT images of calvarial bone defects at 4 and 8 weeks post-treatment across experimental groups. (c)–(f) Quantitative analysis of BV/TV (%), Tb.Th, Tb.N, and Tb.Sp in calvarial bone defects among different treatment groups. ns means no significant, * $P < 0.05$, ** $P < 0.01$, *** $P < 0.001$, and **** $P < 0.0001$.

performed HE staining and Masson's trichrome staining. At 4 and 8 weeks post-treatment, the bone sections from the scaffold + Aged + Mito(Y) hPDLSCs group exhibited a significant increase in new bone formation and osteoid matrix deposition, demonstrating bone-forming capabilities similar to those of the scaffold + Young hPDLSCs group. In contrast, the scaffold + Aged + shAKAP1 Mito(Y) hPDLSCs group, in which AKAP1 was knocked down, showed markedly reduced new bone formation. Moreover, new bone formation displayed a time-dependent trend (Figs. 8(a) and 8(b)). Collectively, these findings indicate that mitochondrial supplementation therapy holds substantial potential for enhancing endogenous bone regeneration.

3 Discussion

Characterized by the gradual accumulation of molecular and cellular damage, aging is a progressive process primarily mediated by the activation of the p53-p21 or p16-Rb pathways [34]. During aging, bone homeostasis is frequently disrupted, leading to reduced bone turnover rates and increased bone marrow adiposity, and ultimately contributing to age-related bone diseases such as osteoporosis [42, 43]. It has been demonstrated that aging impairs the osteogenic potential of BMSCs, disrupting the bone-fat balance and thereby diminishing bone formation [44]. In the field of periodontal regeneration, studies have shown that the resorption and destruction of alveolar bone are more pronounced in aged individuals, further highlighting the negative impact of aging on osteogenesis [45]. Consistent with these findings, our study confirmed significant maxillary bone mass loss in aged mice, and *in vitro* experiments revealed that aging markedly weakens the osteogenic differentiation capacity of hPDLSCs.

Mitochondria, known as the "powerhouses" of cells, play a

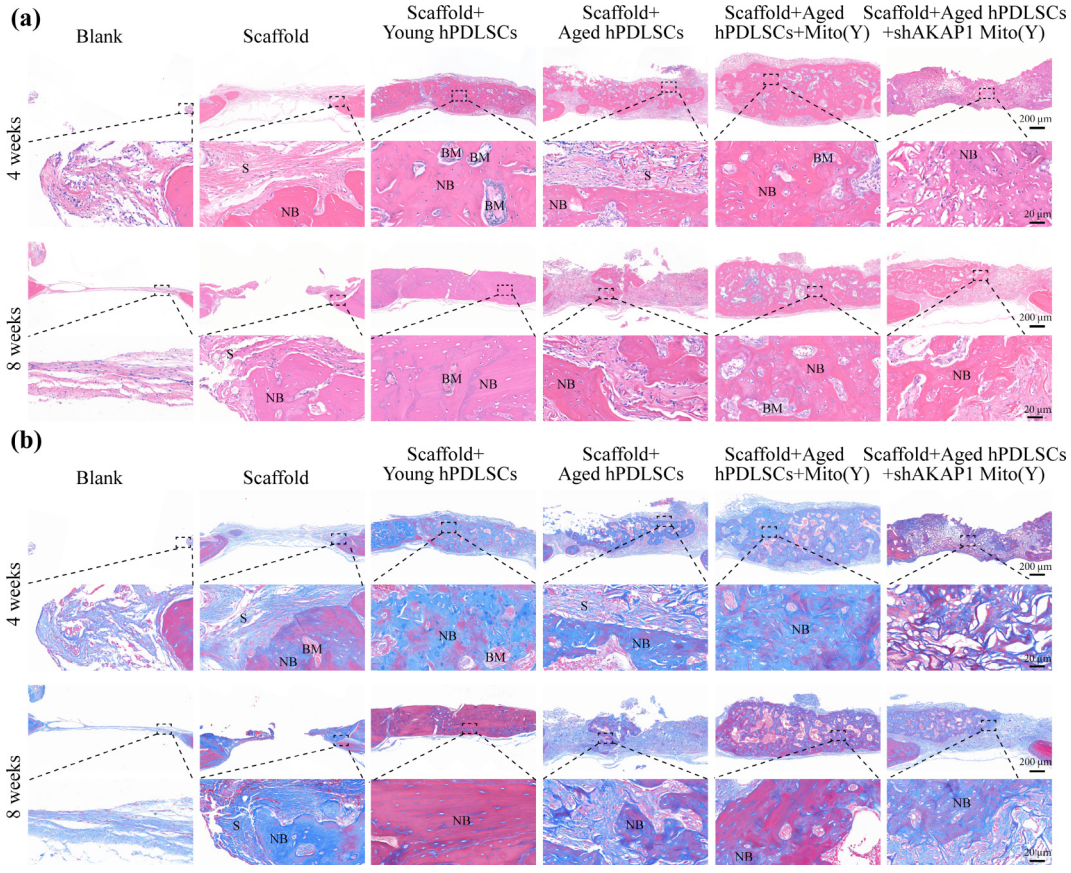

Figure 8 HE, Masson staining, and IF of calvarial bone regeneration. (a) HE staining of calvarial bone defects at 4 and 8 weeks post-treatment across experimental groups (NB: new bone; S: scaffold; BM: bone marrow). (b) Masson staining of calvarial bone defects at 4 and 8 weeks post-treatment across experimental groups.

central role in cellular energy production, and their dysfunction is recognized as one of the hallmarks of aging [46]. Mitochondrial dysfunction is frequently associated with elevated levels of ROS, decreased $\Delta\Psi_m$, and reduced ATP production, significantly impairing mitochondrial homeostasis and contributing to various bone diseases [47]. Recent studies have demonstrated that the overexpression of mitochondrial antioxidant enzymes, including manganese superoxide dismutase (MnSOD), methionine sulfoxide reductase, and catalase, can extend lifespan [48–50]. Similarly, research has demonstrated that enhancing mitochondrial antioxidant capacity can reduce ROS production, thereby maintaining mitochondrial homeostasis and promoting longevity [51]. This supports the conclusion that excessive ROS production in mitochondria leads to mitochondrial dysfunction and subsequently contributes to aging. Our data demonstrate that aged hPDLSCs exhibit abnormal mitochondrial morphology, functional decline, and diminished osteogenic differentiation capacity. These indicate that mitochondrial dysfunction is a major cause of osteogenic damage, and restoring mitochondrial function may represent a promising therapeutic strategy for recovering osteogenesis.

In recent years, studies have demonstrated that mitochondria replenishment can serve as an effective strategy to restore osteogenic capacity [35]. Extensive research has also confirmed that mitochondria can be transferred between various cell types to enhance the metabolic and proliferative functions of damaged or cancerous cells [47, 52]. Healthy bone resident cells can transfer mitochondria to neighboring cells under metabolic stress, thereby restoring their metabolic function and maintaining bone homeostasis. The mechanism involves upregulating mitochondrial fusion protein 2 (Mfn2), whose expression declines with age [53]. Another study on BMSCs has demonstrated that BMSCs can activate the Wnt/β-Catenin signaling through mtDNA transfer, thereby promoting bone regeneration in a high-salt microenvironment [54]. Similarly, pre-transplantation autologous mitochondrial transfer to BMSCs significantly enhances their proliferation, osteogenic differentiation, angioblast, and migratory capabilities. Furthermore, mitochondrial transfer upregulates oxidative phosphorylation (OXPHOS) activity and mitochondrial ATP production. Animal experiments have also confirmed that mitochondrial transfer accelerates the BMSCs-mediated bone defect healing process [35, 55]. However, investigations into mitochondria replenishment in hPDLSCs remain limited, particularly studies on the efficient extraction of mitochondria for transfer to recipient cells. Therefore, we explored the potential of restoring mitochondrial function and osteogenic differentiation capacity in aged hPDLSCs through mitochondria replenishment. Our experimental results validate the feasibility of using mitochondrial replenishment strategy to rejuvenate sencesent stem cell and promote bone defect repair.

Mitochondrial integrity is essential for maintaining cellular energy homeostasis, calcium buffering, and apoptosis regulation. Throughout the experiment, we employed 4 °C low-temperature centrifugation to minimize the risk of mitochondrial degradation caused by external factors. The isolated mitochondria were immediately suspended in a mitochondrial storage buffer to ensure optimal stability during *in vitro* storage. One limitation of this study

is the lack of direct measurements of mitochondrial parameters, such as oxygen consumption rate and cytochrome c (Cyt c) release, during storage. Future work will integrate real-time monitoring with the Seahorse XF Analyzer to quantify storage-induced mitochondrial stress and optimize preservation protocols.

Studies have shown that isolated mitochondria lack intact nuclear DNA and major histocompatibility complex (MHC) molecules, thereby exhibiting relatively low immunogenicity. Autologous mitochondrial transplantation generally does not result in elevated levels of inflammation-related cytokines or significant immune or inflammatory responses [56]. However, under prolonged co-culture conditions, mtDNA leakage due to mitochondrial damage or lysis post-transplantation may trigger an immune response via the TLR9 pathway [57]. Therefore, future research should focus on assessing mitochondrial supplementation induces immunogenic reactions and quantifying the levels of pro-inflammatory cytokines (such as IL-6 and TNF-α) following transplantation and explore mtDNA removal or encapsulation strategies to enhance biocompatibility.

In conclusion, this research demonstrates that transferring mitochondria from young hPDLSCs to aged hPDLSCs can significantly improve mitochondrial function, restore $\Delta\Psi_m$ levels, and reduce ROS production. More importantly, this process markedly enhances the osteogenic capacity of aged hPDLSCs. Additionally, we found that mitochondria replenishment upregulates the expression of the mitochondrial-anchored protein AKAP1, which activates the cAMP/PKA signaling pathway and regulates mitochondrial homeostasis. These findings indicate that mitochondrial supplementation therapy holds great promise for restoring the function of aging cells.

Despite verifying the significant effects of mitochondria replenishment on aged hPDLSCs, our study has certain limitations. The research primarily focused on the role of the cAMP/PKA signaling pathway in mitochondrial function recovery and osteogenic differentiation but did not delve into specific downstream mechanisms. Furthermore, future studies should explore methods to achieve efficient and large-scale mitochondria replenishment to facilitate clinical application. Simultaneously, increased focus on the *in vitro* preservation technology of mitochondria and artificial mitochondria research and development is anticipated to further broaden the application prospects of stem cell therapy.

4 Conclusion

This study systematically elucidated the mechanisms by which mitochondrial dysfunction in aged hPDLSCs contributes to reduced osteogenic differentiation capacity and verified the feasibility of restoring their function through mitochondria replenishment. The results demonstrated that mitochondrial supplementation therapy significantly improved mitochondrial function and restored osteogenic differentiation ability by upregulating the expression of mitochondrial-anchored protein AKAP1 and activating the cAMP/PKA signaling pathway. This discovery not only provides a critical theoretical foundation for bone regeneration but also opens new avenues for treating age-related diseases. Future research will focus on unraveling more complex regulatory networks and developing efficient mitochondria replenishment technologies to facilitate the clinical translation of this strategy.

5 Materials and methods

5.1 Cell culture and treatment

hPDLSCs were isolated from the periodontal ligament tissues of permanent teeth extracted from patients with orthodontic demands at the Department of Orthodontics, Tongji Hospital, affiliated with Tongji Medical College, Huazhong University of Science and Technology. This study protocol got permission from the ethics committee (Ethics number: TJ-IRB202502070). The middle third of the tooth root were scraped to obtain periodontal ligament and subsequently digested at 37 °C for 1.5 h by the mixture of 2 mg/mL collagenase type I (Thermofisher, USA) and 1 mg/mL dispase II (Yeasen, China). Then the mixture was centrifuged at 1000 rpm for 5 min. The sedimentary cells were collected and inoculated into T25 cell culture flasks using MEM-α (Boster, China) supplemented with 20% fetal bovine serum (Boster, China) and 1% penicillin-streptomycin (Servicebio, China). The culture flasks were placed in the incubator at 37 °C in a moist atmosphere containing 5% CO_2. The medium was substituted to fresh medium every 2 days. The fetal bovine content was changed to 10% after the first passaging. In this experiment, aged hPDLSCs were generated using serial passaging. Young hPDLSCs were defined as those in passages 2–5, while aged hPDLSCs were identified as those in passages 10–15. Throughout the experiment, exposure of cells and mitochondria to EDTA was avoided.

5.2 Mitochondria isolation

When the cell density of young hPDLSCs cultured in the T25 cell culture flasks reached approximately 90%, mitochondria were isolated by the Mitochondrial Isolation Kit (Beyotime, China). The mitochondria and cytoplasmic fractions were separated through differential centrifugation steps under the guidance of the instruction. Before being transferred, the isolated mitochondria were stored on ice in the complete culture medium. After thoroughly discarding the supernatant of aged hPDLSCs (receivers), the mitochondrial suspension was gradually introduced dropwise. The receiver hPDLSCs and the transferred mitochondria were incubated at 37 °C for 24 h before proceeding with subsequent experiments.

5.3 Cell proliferation analysis

hPDLSCs were inoculated to a 6-well plate with 2×10^5 cells per well. The EdU Assay Kit (Beyotime, China) was utilized to assess cell proliferation in accordance with the instruction. After incubation, the cells were observed and photographed by the fluorescence microscope (IX 71, Olympus, Japan).

5.4 Transmission electron microscopy

hPDLSCs from a T75 cell culture flask with the density of 90% were collected and fixed with glutaraldehyde in phosphate-buffered solution. Following dehydration, infiltration, embedding, and staining, ultra-thin sections were prepared. The morphology, structure, size, and quantity of mitochondria were detected by the TEM. Multiple field images were captured for analysis.

5.5 JC-1 staining

hPDLSCs were inoculated to a 6-well plate with 2×10^5 cells per well. The JC-1 working solution (Solarbio, China) was prepared under the guidance from manufacturer. The cells were incubated

with the prepared JC-1 staining solution at 37 °C for 20 min in the cell incubator. Then, the staining solution was discarded, and the cells were washed twice using the JC-1 staining buffer. Next, 2 mL culture medium was added to each well. The positive proportion of stained cells was calculated by the flow cytometer (Neon-1026M, Beamcyte, China). The data were processed by the FlowJo software (Tree Star).

5.6 ROS detection

hPDLSCs were inoculated to a 6-well plate with 2×10^5 cells per well. The intracellular ROS levels were detected by the ROS Detection Kit (Beyotime, China) on the basis of the manufacturer's protocol. Briefly, the cells were incubated with DCFH-DA (10 μM) at 37 °C for 20 min and serum-free medium was used to wash cells three times after incubation. The fluorescent cells were observed and photographed by the fluorescence microscope (IX 71, Olympus, Japan) and the flow cytometer (Neon-1026M, Beamcyte, China).

5.7 MitoSOX assay

hPDLSCs were inoculated to a 6-well plate with 2×10^5 cells per well. The MitoSOX probe (Yeasen, China) was utilized to detect the intracellular ROS levels. Cells were incubated with the MitoSOX working solution (500 nM) at 37 °C for 30 min. PBS solution was utilized to wash cells three times after incubation. The fluorescent cells were observed and photographed by the fluorescence microscope (IX 71, Olympus, Japan).

5.8 Lentiviral transfection

The second-generation hPDLSCs were inoculated to a 12-well plate with 1×10^5 cells per well. As the cell confluence reached 30%–40%, TOMM20-GFP lentivirus (Obio, China) was added according to the optimal MOI (MOI = 20). After viral infection for 12–16 h, the culture medium was substituted with 1 mL fresh complete medium per well. Cells were cultured for an additional 72 h until proceeding with subsequent experiments.

5.9 Quantitative real-time polymerase chain reaction

hPDLSCs were inoculated to a 6-well plate with 2×10^5 cells per well. Total RNA was extracted from hPDLSCs by the SteadyPure Quick RNA Extraction Kit (Accurate Biology, China) under the instruction from manufacturer. The total transcriptome cDNA synthesis kit (Accurate Biology, AG11707) was utilized to reverse-transcribe extracted RNA into cDNA. qRT-PCR analysis was conducted using 2×SYBR Green Master Mix (Yeasen, China) on a real-time PCR system (LightCycler 480 Instrument II, Roche, Switzerland) to quantify gene expression. Primer sequences were provided in Table S1 in the ESM.

5.10 Western blot

After subjecting *in vitro*-cultured hPDLSCs to the corresponding treatments, lyse cells by RIPA buffer with 1% protease inhibitor pre-added on ice. The lysates and cells were collected into an EP tube and centrifuged at 12,000 rpm for 20 min with the temperature of 4 °C. Supernatants were collected and a 1/4 volume loading buffer was added to it. The mixture was denatured at 95 °C for 10 min and loaded onto SDS-PAGE gels. Following electrophoresis, proteins were transferred to preactivated PVDF membrane. The membrane was soaked in 5% skim milk at room temperature for 1 h to block. TBST solution was utilized to wash the membrane three times and subsequently the primary antibodies were incubated at 4 °C overnight on an orbital shaker. TBST solution was utilized to wash the membrane three times and the membrane was incubated with HRP-conjugated secondary antibodies at room temperature for 1 h on an orbital shaker. The ECL reagent was utilized to visualize the protein bands. The primary antibodies used were: Runx2 (1:2000; Proteintech), P21(1:1000 Abclonal), ALPL (1:2000; Proteintech), COL-I (1:2000; Proteintech), TOMM20(1:1000 Abclonal), AKAP1 (1:1000; Proteintech), P16(1:1000; Abclonal), and β-actin (1:1000; CST).

5.11 ALP and ARS

hPDLSCs were inoculated to a 6-well plate with 2×10^5 cells per well. The culture was substituted to the osteogenic medium when cell density reached 40%–60%. The osteogenic medium contained 10% FBS, 1% penicillin/streptomycin, 50 μg/mL ascorbic acid, 10 mM β-glycerophosphate dissolved in Dulbecco's modified Eagle medium (DMEM, Servicebio, China). Cells were fixed and stained for ALP (Beyotime, China) and ARS staining (Beyotime, China) after culturing 7 and 21 days.

5.12 shRNA-mediated gene silencing

shRNA lentiviral particles targeting human AKAP1 (Wuhan Puyun Biotechnology Co., Ltd.) were obtained. Cells were transfected using Lipofectamine 2000 (Thermo Fisher) and cells were collected after 48 h of culture. mRNA was isolated from the transfected cells and quantitative PCR and qRT-PCR were performed to verify the shRNA silencing efficiency.

5.13 RNA-seq

The sequencing groups were classified as: Young hPDLSCs, Aged hPDLSCs, and Aged + Mito(Y) hPDLSCs. RNA sequencing analysis was conducted on three RNA samples from each group at Shanghai Majorbio Bio-pharm Technology Co., Ltd. (China). The total RNA was extracted by MJZol total RNA ext method, and the purity and concentration of the RNA were detected using Nanodrop2000. The integrity of RNA was assessed through agarose gel electrophoresis, and the RNA integrity number (RIN) was calculated by Agilent5300. Libraries were prepared using the SMART-Seq v4 Ultra Low Input RNA Kit for Sequencing protocol, followed by PCR amplification and purification. An Illumina NovaSeq X Plus platform was utilized to perform sequencing. RNA-seq data were finally deposited in the GEO database (PRJNA1207513).

5.14 Mouse maxillary bone model

To evaluate the differences in maxillary bone mass between young and aged mice, maxillae were collected from female C57BL/6 mice (8 weeks and 15 months old, nearly 20 and 30 g weight, respectively). The experimental protocol got permission from the animal ethics committee of Tongji Hospital, Tongji Medical College, Huazhong University of Science and Technology (No.TJH-202408008). C57BL/6 mice were purchased from Beijing Vital River Laboratory Animal Technology Co., Ltd. (China). Each group consisted of five mice. The mice were euthanized, and their maxillae were separated. The specimens were steeped in 4% paraformaldehyde for 24 h to fix and utilize a micro-CT system (Skyscan 1176, Bruker) to scan and assess the differences of maxillary bone mass between young and aged mice.

5.15 Scaffold preparation

A biomimetic scaffold was fabricated through the co-assembly and intrafibrillar mineralization of collagen fibrils and ZnO nanowires (IMC/ZnO) [58, 59]. Briefly, 0.05 mg/mL of ZnO nanowires was co-assembled with type I collagen solution (Corning, USA) at 37 °C for 24 h. Three-dimensional (3D) porous scaffolds were formed by pouring the collagen-ZnO composite into molds, followed by freezing and lyophilization. Then the scaffold was crosslinked by N-hydroxysuccinimide and 1-ethyl-3-(3-dimethylaminopropyl)-carbodiimidec for 4 h and mineralized in a solution containing K_2HPO_4, $CaCl_2$, and polyaspartic acid for 3–5 days.

5.16 Establishment of a rat calvarial defect model

Rat models (Sprague-Dawley rats, male, 6–8 weeks old, 200–220 g) with calvarial defect were created to the bone regeneration effect of mitochondria replenishment. The experimental protocol got permission from the animal ethics committee of Tongji Hospital, Tongji Medical College, Huazhong University of Science and Technology (No. TJH-202407041). 1% pentobarbital sodium solution was prepared for intraperitoneal injection to anesthetize the rats. A trephine was utilized to make the circular and critical-sized defect (diameter = 5 mm) in the calvaria. Then, the rats were assigned randomly to the following treatment groups, each group consisted of at least six mice: (1) blank group, (2) Scaffold, (3) Scaffold loaded with young PDLSCs, (4) Scaffold loaded with Aged PDLSCs, (5) Scaffold loaded with Aged + Mito(Y), and (6) Scaffold loaded with Aged + shAKAP1 Mito(Y). The scaffolds were trimmed in order to fit the sizes of the defects and then implanted. The wound was closed by meticulously suturing the periosteum and skin. Four or eight weeks later, the rats were euthanized and the calvaria was striped. The specimens were steeped in 4% paraformaldehyde for 24 h to fix and utilize a micro-CT system (Skyscan 1176, Bruker) to assess the scales of the bone regeneration within the defects.

5.17 Histological staining assessment

The samples of mice maxillary and rat calvarial were soaked in 4% neutral buffered formalin for 24 h to fix. Then, the sample was transferred to 15% EDTA (pH 7.4) for 4 weeks to be decalcified. The decalcification solution was changed every 2 days. The tissue was then trimmed and complete decalcification, embedded in paraffin, and sectioned for histological analysis through hematoxylin-eosin and Masson staining. For immunohistochemical staining, the paraffin sections were dewaxed and the 5% normal goat serum was utilized to block them at room temperature for 30 min. The primary antibodies were incubated overnight at 4 °C. The primary antibodies used were: Runx2 (1:200; ABclonal), OPN (1:200; Boster), and OCN (1:200; ABclonal). Following PBS washing, the HRP-conjugated secondary antibodies were utilized to incubate the sections for 1 h. For immunofluorescence staining, the paraffin sections were dewaxed and rehydrated. Soaking in 0.125% trypsin and 20 μg/mL proteinase K at 37 °C for 30 min was performed for antigen retrieval. The sections were permeabilized with 0.1% Triton X-100 within 10 min and blocked by 5% BSA at room temperature within 30 min. The primary antibodies were incubated overnight at 4 °C, including CD146 (1:200; Abcam), Runx2 (1:200; ABclonal), and OCN (1:50; Servicebio). PBS solution was utilized to wash the sections, and incubated with AlexaFluor-conjugated secondary antibodies at room temperature for no less than 1 h. The nuclei were counterstained with DAPI. Fluorescence images were captured through a confocal scanning microscope (Pannoramic SCAN, 3DHISTECH caseviewer). The ratio of positive cells to the total tissue area was measured in four regions per section using ImageJ software (National Institutes of Health, USA) to determine the percentage of positively stained cells.

5.18 Statistical analysis

In order to compare the differences between two groups, independent *t*-tests were conducted. In order to compare the differences among three or more groups, one-way ANOVA was performed followed by Tukey's post hoc multiple comparisons test. The significance level for all statistical tests was set at $P < 0.05$. GraphPad Prism version and 8.0. SPSS version 27.0 were utilized to accomplish the data analysis.

Electronic Supplementary Material: Supplementary material (additional experimental details and data, including characterization of hPDLSCs, establishment of senescence models, validation of mitochondrial extraction and isolation protocols, physicochemical characterization of scaffold materials, comparative analysis of mitochondrial function and osteogenic differentiation capacity pre- and post-AKAP1 knockout, quantification of PKA activity alterations, verification of mitochondrial supplementation efficiency, uncropped Western blot results, primer sequences for qRT-PCR analysis) is available in the online version of this article at https://doi.org/10.26599/NR.2025.94907375.

Data availability

The data supporting the findings of this study are accessible from the corresponding author upon reasonable request. SRA records (PRJNA1207513) of RNA-Seq raw data concerning this study will be accessible with the following link: https://www.ncbi.nlm.nih.gov/sra/PRJNA1207513.

Acknowledgements

This work was financially supported by the Hubei Natural Science Foundation (No. 2025AFB554 (S. Q. G.)), the National Natural Science Foundation of China (No. 82230030 (Y. L.)), the National Key Research and Development Program of China (No. 2024YFA1210400 (Y. L.)), Beijing Natural Science Foundation (No. L234017 (Y. L.)), Key R & D Plan of Ningxia Hui Autonomous Region (No. 2020BCG01001 (Y. L.)), First-Class Discipline Team of Kunming Medical University (No. 2024XKTDTS08 (Y. L.)), and Innovative Research Team of High-level Local Universities in Shanghai (No. SHSMU-ZLCX20212402 (Y. L.)).

We thank for the technical support from the Huazhong University of Science and Technology Analytical & Testing center, Animal Experimental Center, Medical sub-center and Experimental Medicine Center, Tongji Hospital, Tongji Medical College, Huazhong University of Science and Technology.

Declaration of competing interest

All the contributing authors report no conflict of interests in this work.

Author contribution statement

G. N.: Investigation, methodology, writing – original draft. M. Y.:

Methodology. X. Y. W.: Supervision, writing – review & editing. Y. X. Z.: Software. Y. Y. L.: Investigation. K. H. Z.: Investigation. L. P.: Investigation. A. O.: Investigation. Y. X. W.: Investigation. Q. L. L.: Conceptualization. J. M.: Supervision, writing – review & editing. Y. L.: Supervision, writing – review & editing, funding acquisition. S. Q. G.: Conceptualization, supervision, funding acquisition, writing – review & editing. All the authors have approved the final manuscript.

Informed consent

Written informed consent for participation was obtained from the patients.

Ethics statement

The animal experiments were carried out following the guidelines of the animal ethics committee of Tongji Hospital, Tongji Medical College, Huazhong University of Science and Technology (Ethical code: No. TJH-202407041, No.TJH-202408008). The protocol for isolating hPDLSCs from human tissue samples was approved by the Institutional Ethics Committee (Approval Number: TJ-IRB202502070).

Use of AI statement

None.

References

[1] Abou Neel, E. A.; Chrzanowski, W.; Salih, V. M.; Kim, H. W.; Knowles, J. C. Tissue engineering in dentistry. *J. Dent.* **2014**, *42*, 915–928.

[2] Choi, J. W.; Kim, Y. C. Asian facial recontouring surgery. *Plast. Aesthet. Res.* **2023**, *10*, 59.

[3] Autelitano, L.; Meazzini, M. C. Alveolar cleft reconstruction with vomerine bone: Two surgical procedures in one step: A case series. *Plast. Aesthet. Res.* **2023**, *10*, 16.

[4] Xu, Y. R.; Saiding, Q.; Zhou, X.; Wang, J.; Cui, W. G.; Chen, X. L. Electrospun fiber-based immune engineering in regenerative medicine. *Smart Med.* **2024**, *3*, e20230034.

[5] Li, Z. H.; Liu, H. R.; Wang, R.; Ji, C. H.; Wei, Y.; Shi, M. S.; Wang, Y. Q.; Du, Y. P.; Zhang, Y. F.; Yuan, Q. et al. Bioactive core-shell CaF_2 upconversion nanostructure for promotion and visualization of engineered bone reconstruction. *ACS Nano* **2020**, *14*, 16085–16095.

[6] Wang, Y. Q.; Hu, X. X.; Zhang, L. L.; Zhu, C. L.; Wang, J.; Li, Y. X.; Wang, Y. L.; Wang, C.; Zhang, Y. F.; Yuan, Q. Bioinspired extracellular vesicles embedded with black phosphorus for molecular recognition-guided biomineralization. *Nat. Commun.* **2019**, *10*, 2829.

[7] Liu, Z. Y.; Guo, C. B.; Guo, J.; Huang, S.; Du, P. Research progress on application of dental stem cells in alveolar bone and periodontal regeneration. *MedComm Future Med.* **2024**, *3*, e98.

[8] Wang, R.; Liao, L.; Huang, X. J.; Ma, S. X.; Wang, S.; Qiao, H.; Zhou, H.; Zou, J.; Su, X. X. Mechano-responsive microRNA-functionalized PDLSC exosomes as a novel therapeutic for inflammatory bone loss in periodontitis. *Chem. Eng. J.* **2023**, *458*, 141488.

[9] Lei, Y.; Zhang, Q. F.; Kuang, G. Z.; Wang, X. C.; Fan, Q. H.; Ye, F. F. Functional biomaterials for osteoarthritis treatment: From research to application. *Smart Med.* **2022**, *1*, e20220014.

[10] Stolzing, A.; Jones, E.; McGonagle, D.; Scutt, A. Age-related changes in human bone marrow-derived mesenchymal stem cells: Consequences for cell therapies. *Mech. Ageing Dev.* **2008**, *129*, 163–173.

[11] Lin, H.; Sohn, J.; Shen, H.; Langhans, M. T.; Tuan, R. S. Bone marrow mesenchymal stem cells: Aging and tissue engineering applications to enhance bone healing. *Biomaterials* **2019**, *203*, 96–110.

[12] Goodell, M. A.; Rando, T. A. Stem cells and healthy aging. *Science* **2015**, *350*, 1199–1204.

[13] Rudolph, K. L. Stem cell aging. *Mech. Ageing Dev.* **2021**, *193*, 111394.

[14] Iwata, T.; Yamato, M.; Washio, K.; Yoshida, T.; Tsumanuma, Y.; Yamada, A.; Onizuka, S.; Izumi, Y.; Ando, T.; Okano, T. et al. Periodontal regeneration with autologous periodontal ligament-derived cell sheets - A safety and efficacy study in ten patients. *Regen. Ther.* **2018**, *9*, 38–44.

[15] Zhang, J.; An, Y.; Gao, L. N.; Zhang, Y. J.; Jin, Y.; Chen, F. M. The effect of aging on the pluripotential capacity and regenerative potential of human periodontal ligament stem cells. *Biomaterials* **2012**, *33*, 6974–6986.

[16] Logan, D. C. The mitochondrial compartment. *J. Exp. Bot.* **2006**, *57*, 1225–1243.

[17] Niizuma, K.; Yoshioka, H.; Chen, H.; Kim, G. S.; Jung, J. E.; Katsu, M.; Okami, N.; Chan, P. H. Mitochondrial and apoptotic neuronal death signaling pathways in cerebral ischemia. *Biochim. Biophys. Acta (BBA)-Mol. Basis Dis.* **2010**, *1802*, 92–99.

[18] Suh, J.; Kim, N. K.; Shim, W.; Lee, S. H.; Kim, H. J.; Moon, E.; Sesaki, H.; Jang, J. H.; Kim, J. E.; Lee, Y. S. Mitochondrial fragmentation and donut formation enhance mitochondrial secretion to promote osteogenesis. *Cell Metab.* **2023**, *35*, 345–360.e7.

[19] Huang, T.; Lin, R. Y.; Su, Y. Q.; Sun, H.; Zheng, X. X.; Zhang, J. S.; Lu, X. Y.; Zhao, B. Q.; Jiang, X. C.; Huang, L. L. et al. Efficient intervention for pulmonary fibrosis via mitochondrial transfer promoted by mitochondrial biogenesis. *Nat. Commun.* **2023**, *14*, 5781.

[20] Wei, B.; Ji, M. L.; Lin, Y. C.; Wang, S. Z.; Liu, Y. X.; Geng, R.; Hu, X. Y.; Xu, L.; Li, Z.; Zhang, W. T. et al. Mitochondrial transfer from bone mesenchymal stem cells protects against tendinopathy both *in vitro* and *in vivo*. *Stem Cell Res. Ther.* **2023**, *14*, 104.

[21] Zhang, K. H.; Li, Q. L.; Zhang, Y. X.; Nuerlan, G.; Li, Y. Y.; Mao, J.; Gong, S. Q. Targeting mitophagy as a potential therapeutic approach for age-related bone diseases. *Adv. Ther.* **2024**, *7*, 2400078.

[22] Quan, Y.; Xin, Y. G.; Tian, G.; Zhou, J. T.; Liu, X. J. Mitochondrial ROS-modulated mtDNA: A potential target for cardiac aging. *Oxid. Med. Cell. Longev.* **2020**, *2020*, 9423593.

[23] Bratic, A.; Larsson, N. G. The role of mitochondria in aging. *J. Clin. Invest.* **2013**, *123*, 951–957.

[24] Nitzan, K.; Benhamron, S.; Valitsky, M.; Kesner, E. E.; Lichtenstein, M.; Ben-Zvi, A.; Ella, E.; Segalstein, Y.; Saada, A.; Lorberboum-Galski, H. et al. Mitochondrial transfer ameliorates cognitive deficits, neuronal loss, and gliosis in Alzheimer's disease mice. *J. Alzheimers Dis.* **2019**, *72*, 587–604.

[25] Zhang, A. L.; Liu, Y. Y.; Pan, J. N.; Pontanari, F.; Chia-Hao Chang, A.; Wang, H. H.; Gao, S.; Wang, C. Q.; Chang, A. C. Delivery of mitochondria confers cardioprotection through mitochondria replenishment and metabolic compliance. *Mol. Ther.* **2023**, *31*, 1468–1479.

[26] Lin, M. T.; Beal, M. F. Mitochondrial dysfunction and oxidative stress in neurodegenerative diseases. *Nature* **2006**, *443*, 787–795.

[27] Borcherding, N.; Brestoff, J. R. The power and potential of mitochondria transfer. *Nature* **2023**, *623*, 283–291.

[28] Liu, D. L.; Gao, Y. S.; Liu, J.; Huang, Y. G.; Yin, J. H.; Feng, Y. Y.; Shi, L. J.; Meloni, B. P.; Zhang, C. Q.; Zheng, M. H. et al. Intercellular mitochondrial transfer as a means of tissue revitalization. *Signal Transduct. Target. Ther.* **2021**, *6*, 65.

[29] Seo, B. M.; Miura, M.; Gronthos, S.; Mark Bartold, P.; Batouli, S.; Brahim, J.; Young, M.; Gehron Robey, P.; Wang, C. Y.; Shi, S. T. Investigation of multipotent postnatal stem cells from human periodontal ligament. *Lancet* **2004**, *364*, 149–155.

[30] Lei, F. Z.; Li, M. J.; Lin, T. T.; Zhou, H.; Wang, F.; Su, X. X.

Treatment of inflammatory bone loss in periodontitis by stem cell-derived exosomes. *Acta Biomater.* **2022**, *141*, 333–343.
[31] Tan, Y. Z.; Xu, X. Y.; Dai, J. M.; Yin, Y.; He, X. T.; Zhang, Y. L.; Zhu, T. X.; An, Y.; Tian, B. M.; Chen, F. M. Melatonin induces the rejuvenation of long-term *ex vivo* expanded periodontal ligament stem cells by modulating the autophagic process. *Stem Cell Res. Ther.* **2021**, *12*, 254.
[32] Konstantonis, D.; Papadopoulou, A.; Makou, M.; Eliades, T.; Basdra, E. K.; Kletsas, D. Senescent human periodontal ligament fibroblasts after replicative exhaustion or ionizing radiation have a decreased capacity towards osteoblastic differentiation. *Biogerontology* **2013**, *14*, 741–751.
[33] Hu, M. L.; Liu, R. Q.; Chen, X. Y.; Yan, S.; Gao, J.; Zhang, Y.; Wu, D.; Sun, L.; Jia, Z.; Sun, G. Y. H. et al. Metabolomics dysfunction in replicative senescence of periodontal ligament stem cells regulated by AMPK signaling pathway. *Stem Cells Dev.* **2024**, *33*, 607–615.
[34] López-Otín, C.; Blasco, M. A.; Partridge, L.; Serrano, M.; Kroemer, G. The hallmarks of aging. *Cell* **2013**, *153*, 1194–1217.
[35] Guo, Y. S.; Chi, X. P.; Wang, Y. F.; Heng, B. C.; Wei, Y.; Zhang, X. H.; Zhao, H.; Yin, Y.; Deng, X. L. Mitochondria transfer enhances proliferation, migration, and osteogenic differentiation of bone marrow mesenchymal stem cell and promotes bone defect healing. *Stem Cell Res. Ther.* **2020**, *11*, 245.
[36] Islam, M. N.; Das, S. R.; Emin, M. T.; Wei, M.; Sun, L.; Westphalen, K.; Rowlands, D. J.; Quadri, S. K.; Bhattacharya, S.; Bhattacharya, J. Mitochondrial transfer from bone-marrow-derived stromal cells to pulmonary alveoli protects against acute lung injury. *Nat. Med.* **2012**, *18*, 759–765.
[37] Omura, T. Mitochondria-targeting sequence, a multi-role sorting sequence recognized at all steps of protein import into mitochondria. *J. Biochem.* **1998**, *123*, 1010–1016.
[38] Tröger, J.; Moutty, M. C.; Skroblin, P.; Klussmann, E. A-kinase anchoring proteins as potential drug targets. *Br. J. Pharmacol.* **2012**, *166*, 420–433.
[39] Zaccolo, M.; Zerio, A.; Lobo, M. J. Subcellular organization of the cAMP signaling pathway. *Pharmacol. Rev.* **2021**, *73*, 278–309.
[40] Taskén, K.; Aandahl, E. M. Localized effects of cAMP mediated by distinct routes of protein kinase A. *Physiol. Rev.* **2004**, *84*, 137–167.
[41] Zhang, Y. X.; Li, Z. X.; Guo, B. W.; Wang, Q. B.; Chen, L. Y.; Zhu, L. S.; Zhang, T.; Wang, R. X.; Li, W. R.; Luo, D. et al. A zinc oxide nanowire-modified mineralized collagen scaffold promotes infectious bone regeneration. *Small* **2024**, *20*, 2309230.
[42] Li, C. J.; Xiao, Y.; Yang, M.; Su, T.; Sun, X.; Guo, Q.; Huang, Y.; Luo, X. H. Long noncoding RNA Bmncr regulates mesenchymal stem cell fate during skeletal aging. *J. Clin. Invest.* **2018**, *128*, 5251–5266.
[43] Yu, B.; Huo, L. H.; Liu, Y. S.; Deng, P.; Szymanski, J.; Li, J.; Luo, X. H.; Hong, C.; Lin, J. D.; Wang, C. Y. PGC-1α controls skeletal stem cell fate and bone-fat balance in osteoporosis and skeletal aging by inducing TAZ. *Cell Stem Cell* **2018**, *23*, 193–209.e5.
[44] Li, C. J.; Xiao, Y.; Sun, Y. C.; He, W. Z.; Liu, L.; Huang, M.; He, C.; Huang, M.; Chen, K. X.; Hou, J. et al. Senescent immune cells release grancalcin to promote skeletal aging. *Cell Metab.* **2021**, *33*, 1957–1973.e6.
[45] Chen, S. J.; Zhou, D.; Liu, O. S.; Chen, H.; Wang, Y. H.; Zhou, Y. Y. Cellular senescence and periodontitis: Mechanisms and therapeutics. *Biology (Basel)* **2022**, *11*, 1419.
[46] van der Rijt, S.; Molenaars, M.; McIntyre, R. L.; Janssens, G. E.; Houtkooper, R. H. Integrating the hallmarks of aging throughout the tree of life: A focus on mitochondrial dysfunction. *Front. Cell Dev. Biol.* **2020**, *8*, 594416.
[47] Cai, W. J.; Zhang, J. L.; Yu, Y. Q.; Ni, Y. Q.; Wei, Y.; Cheng, Y. H.; Han, L. T.; Xiao, L. Y.; Ma, X. X.; Wei, H. J. et al. Mitochondrial transfer regulates cell fate through metabolic remodeling in osteoporosis. *Adv. Sci. (Weinh.)* **2023**, *10*, 2204871.
[48] Sun, J. T.; Folk, D.; Bradley, T. J.; Tower, J. Induced overexpression of mitochondrial Mn-superoxide dismutase extends the life span of adult *Drosophila melanogaster*. *Genetics* **2002**, *161*, 661–672.
[49] Ruan, H. Y.; Tang, X. D.; Chen, M. L.; Joiner, M. A.; Sun, G. R.; Brot, N.; Weissbach, H.; Heinemann, S. H.; Iverson, L.; Wu, C. F. et al. High-quality life extension by the enzyme peptide methionine sulfoxide reductase. *Proc. Natl. Acad. Sci. USA* **2002**, *99*, 2748–2753.
[50] Schriner, S. E.; Linford, N. J.; Martin, G. M.; Treuting, P.; Ogburn, C. E.; Emond, M.; Coskun, P. E.; Ladiges, W.; Wolf, N.; Van Remmen, H. et al. Extension of murine life span by overexpression of catalase targeted to mitochondria. *Science* **2005**, *308*, 1909–1911.
[51] Andreyev, A. Y.; Kushnareva, Y. E.; Starkov, A. A. Mitochondrial metabolism of reactive oxygen species. *Biochemistry* **2005**, *70*, 200–214.
[52] Lin, R. Z.; Im, G. B.; Luo, A. C.; Zhu, Y. L.; Hong, X. C.; Neumeyer, J.; Tang, H. W.; Perrimon, N.; Melero-Martin, J. M. Mitochondrial transfer mediates endothelial cell engraftment through mitophagy. *Nature* **2024**, *629*, 660–668.
[53] Gao, J. J.; Qin, A.; Liu, D. L.; Ruan, R.; Wang, Q. Y.; Yuan, J.; Cheng, T. S.; Filipovska, A.; Papadimitriou, J. M.; Dai, K. et al. Endoplasmic reticulum mediates mitochondrial transfer within the osteocyte dendritic network. *Sci. Adv.* **2019**, *5*, eaaw7215.
[54] Wang, Y. M.; Lin, S.; Chen, L. J.; Li, M. Z.; Zhu, Z. L.; Zhuang, Z. M.; Cai, M. L.; Zhang, H.; Xing, C. Y.; Li, W. R. et al. Mitochondrial components transferred by MSC-derived exosomes promoted bone regeneration under high salt microenvironment via DRP1/Wnt signaling. *Nano Res.* **2024**, *17*, 8301–8315.
[55] Wang, Y. F.; Li, W. J.; Guo, Y. S.; Huang, Y.; Guo, Y. R.; Song, J.; Mei, F.; Liao, P. W.; Gong, Z. J.; Chi, X. P. et al. Mitochondria transplantation to bone marrow stromal cells promotes angiogenesis during bone repair. *Adv. Sci. (Weinh.)* **2024**, *11*, 2403201.
[56] McCully, J. D.; Cowan, D. B.; Emani, S. M.; del Nido, P. J. Mitochondrial transplantation: From animal models to clinical use in humans. *Mitochondrion* **2017**, *34*, 127–134.
[57] Zhang, Q.; Raoof, M.; Chen, Y.; Sumi, Y.; Sursal, T.; Junger, W.; Brohi, K.; Itagaki, K.; Hauser, C. J. Circulating mitochondrial DAMPs cause inflammatory responses to injury. *Nature* **2010**, *464*, 104–107.
[58] Shao, C. Y.; Zhao, R. B.; Jiang, S. Q.; Yao, S. S.; Wu, Z. F.; Jin, B.; Yang, Y. L.; Pan, H. H.; Tang, R. K. Citrate improves collagen mineralization via interface wetting: A physicochemical understanding of biomineralization control. *Adv. Mater.* **2018**, *30*, 1704876.
[59] Liu, Y.; Li, N.; Qi, Y. P.; Dai, L.; Bryan, T. E.; Mao, J.; Pashley, D. H.; Tay, F. R. Intrafibrillar collagen mineralization produced by biomimetic hierarchical nanoapatite assembly. *Adv. Mater.* **2011**, *23*, 975–980.

This is an open access article under the terms of the Creative Commons Attribution 4.0 International License (CC BY 4.0, https://creativecommons.org/licenses/by/4.0/).

© The Author(s) 2025. Published by Tsinghua University Press.